Heterodyne detection at near-infrared wavelengths with a superconducting NbN hot-electron bolometer mixer

Yury Lobanov,[1,2,*] Michael Shcherbatenko,[1,2] Alexander Shurakov,[1] Alexander V. Rodin,[2,3]
Artem Klimchuk,[2] Alexander I. Nadezhdinsky,[4] Sergey Maslennikov,[1] Pavel Larionov,[1]
Matvey Finkel,[1,5] Alexander Semenov,[1] Aleksandr A. Verevkin,[5] Boris M. Voronov,[1]
Yakov Ponurovsky,[4] Teunis M. Klapwijk,[1,6] and Gregory N. Gol'tsman[1,7]

[1]*Moscow State Pedagogical University, Moscow 119991, Russia*

[2]*Moscow Institute of Physics and Technology (State University), Moscow 141707, Russia*

[3]*Space Research Institute, Russian Academy of Sciences, Moscow 117997, Russia*

[4]*Prokhorov General Physics Institute, Russian Academy of Sciences, Moscow 119991, Russia*

[5]*CSJC "Superconducting Nanotechnology," Moscow 119021, Russia*

[6]*Kavli Institute of NanoScience, Faculty of Applied Sciences, Delft University of Technology,
Lorentzweg 1, 2628 CJ Delft, The Netherlands*

[7]*National Research University Higher School of Economics, 20 Myasnitskaya St., Moscow 101000, Russia*
*Corresponding author: ylobanov@rplab.ru

We report on the development of a highly sensitive optical receiver for heterodyne IR spectroscopy at the communication wavelength of 1.5 μm (200 THz) by use of a superconducting hot-electron bolometer. The results are important for the resolution of narrow spectral molecular lines in the near-IR range for the study of astronomical objects, as well as for quantum optical tomography and fiber-optic sensing. Receiver configuration as well as fiber-to-detector light coupling designs are discussed. Light absorption of the superconducting detectors was enhanced by nano-optical antennas, which were coupled to optical fibers. An intermediate frequency (IF) bandwidth of about 3 GHz was found in agreement with measurements at 300 GHz, and a noise figure of about 25 dB was obtained that was only 10 dB above the quantum limit.   © 2014 Optical Society of America

Heterodyne detection is a commonly used technique in the microwave and terahertz frequency range where high sensitivity and high spectral resolution are needed. However, there are various fields of interest within the IR frequency range where such a technique is also desirable. In astrophysics, IR range observations play a crucial role because the data provide important information about galaxy formation, the evolution of objects in the Universe, and, in particular, possible biochemical processes on Earth-like planets [1–3]. In our galaxy, IR observations can also reveal processes taking place in the atmospheres of the planets and of the Sun [4,5]. Advanced sensitivity in the IR spectrum range will allow detection of molecules such as CO, CO_2, NO_2, NH_3, CH_4, C_2H_2, and others at low concentrations and will facilitate isotope analyses and doppler measurements of the velocity field. Precisely measured profiles of the spectral lines will allow reconstruction of the vertical temperature and gas concentration distributions. Various other scientific applications require both high sensitivity and high resolution IR detection, such as applications used in quantum optical tomography [6–8], optical coherent tomography [9,10], or distributed fiber-optic sensing [11–13]. Since the heterodyne technique comes from radio-astronomy, first attempts were made in the far- and mid-IR range [5,14–16]. Recently, a new approach in using heterodyne detection at 1.55 μm has been introduced [17]. In this approach, a periodically swept tunable fiber-coupled diode laser was used as a local oscillator (LO) source and a PIN-diode was used to detect the signal mixed in an intermediate frequency (IF) bandwidth of 1 MHz.

In this Letter, we demonstrate heterodyne spectroscopy at the communication wavelength of 1.55 μm using superconducting hot-electron bolometer (HEB) mixers [18] with a relatively wide IF bandwidth of about 3 GHz and a sensitivity approaching the quantum limit. The HEB mixers are widely used as receivers at terahertz frequencies [19–24]. Unlike a superconductor–insulator–superconductor (SIS) mixer [25], the HEB mixer does not have an identified upper frequency limit because its principle of operation relies on absorption of radiation by the electrons, which leads to a modulation of the electron temperature at the IF frequency [26]. Operation up to 5.25 THz has been shown [27]. In addition, the noise temperature of the HEB mixer close to the quantum limit $T_N = h\nu/k_B$ has been demonstrated for various frequencies, e.g., Refs. [24,28]. Therefore, it may be possible to use these devices at even higher frequencies of IR wavelengths (on the order of 200 THz) at which a fiber waveguide can be used to guide the radiated power. According to the antenna theorem [29], the maximal effective aperture available in heterodyne detection depends on the wavelength, i.e., $\Omega \cdot S \leq \lambda^2$ where Ω is the fiber efficient field of view, S is the core cross section, and λ is the wavelength. A similar constraint is dictated by the usage of a single mode optical fiber, whose input aperture is

determined by the diffraction and cannot be increased by any front-end optics. Therefore, an optical fiber itself does not limit the performance of heterodyne detection. Moreover, it provides the aperture corresponding to the theoretical limit at the wavelength given. In order to match the absorbing film with the incident radiation, a waveguide mixer-block or a lens in conjunction with a planar antenna is commonly used in the terahertz range. To improve the coupling at IR and optical frequencies a number of optical antennas have been suggested and investigated [30–33]. An optical nanoantenna has also been used with NbN superconducting single photon detectors as well [34]. To enhance the incident light absorption, we made use of Au stripes crossing the NbN bridge, which in turn forms the HEB mixer. As stated in [31], these metals do not conduct very well at optical frequencies and an optical antenna cannot be designed just by scaling its radio frequency analogue with the frequency. Instead, an effective wavelength must be used to determine the scaling factor such that for optical antennas, $2 \leq \lambda/\lambda_{\mathrm{eff}} \leq 6$ [35]; this gives an estimated value for an Au stripe length of 60–220 nm. Each stripe acts as an antenna accumulating incident energy into the nearest pieces of the NbN film, and the whole "zebra" structure helps in absorbing light more efficiently than just a rectangular NbN bridge will. To achieve an efficient coupling, special care is needed to align the polarization of the incident radiation. By means of the isothermal method [36], the absorption coefficient of the "zebra" device was measured to be about 25%, which means that it practically tripled the efficiency compared to the plain NbN bridge efficiency. By varying the length of both the NbN gaps and the Au stripes we have found empirically that the best absorption enhancement (i.e., a relative increase of the measured light absorption coefficient for a given device due to the gold stripe pattern on top of the NbN film) can be achieved with a NbN length of 60 nm and a NbN–NbN–Au period of 120–200 nm. Since the absorbed power depends on the incident power polarization, we suggest that the pattern of gold stripes acts as an optical quasi-antenna [34].

The dimensions of the NbN rectangular bridge are dictated by two contradictory conditions: first, it should be as small as possible to easily provide sufficient LO power needed to set the mixer to the appropriate bias conditions (i.e., where it has the lowest noise and highest gain), and, second, the sensitive element area should approach that of the single mode fiber core diameter, which is ~9 μm for 1.55 μm in standard fibers. Hence, we chose 7 μm as the characteristic size of the sensitive element area. In this case, the device bandwidth (~2.5–3 GHz) is mainly determined by the combination of electron–phonon interactions and phonon to substrate escape times [37]. In fact, a third condition for the geometry of the nanobolometer relates to surface impedance matching. Impedance matching should be achieved for both the incident light to the nanobolometer, as well as for the 50 Ω coaxial line for the IF. These two conditions on impedance matching are difficult to achieve for semiconductor devices. However, for a superconducting device this complication is released because the optical coupling can be simulated and achieved in practice using just an impedance value in the normal state. This

approach is relevant for frequencies $\nu \gg \Delta/h$, where a superconductor impedance approaches its normal state resistance. This could also be justified by ellipsometry measurements [38]. The IF matching can be precisely adjusted to the optimum value of 50 Ω by the proper choice of the LO power and DC biasing of the device.

The devices were made by first forming a NbN–Au bilayer using an *in situ* process, which is important to ensure better electronic contact between the films and avoid possible NbN layer oxidization or contamination. The NbN film was deposited onto an epi-polished surface of a 350-μm thick C-cut sapphire substrate by reactive DC-magnetron sputtering of a Nb target in an Ar-N$_2$ gas mixture (the partial pressure was 5×10^{-3} mbar and 2×10^{-4} mbar for Ar and N$_2$, respectively). The substrate was heated to 800°C and a 4-nm thick NbN film was formed. After the substrate cooled down to 300°C, a 20-nm thick Au layer was formed by DC-magnetron sputtering, also in an Ar atmosphere. Subsequently, the sensitive element was shaped to a 7×7 μm^2 rectangular bridge of the NbN film or to a structure of alternating NbN and NbN–Au stripes by removing the Au selectively (as shown in Fig. 1). These structures were made using ZEP-520A7 resist with e-beam lithography, ion milling, and wet etching (which prevents NbN film damage by the accelerated ions of Ar) of the gold layer. A specially developed mixture of chemicals that does not affect the NbN film properties was used for the gold etching. The width of the bridge was formed with a SiO passivation layer shaped by e-beam lithography and lifted-off of the structure. The Ti–Au–Ti contact pads, which were photolithographically formed on top of the Au small contact pads, served two purposes. Namely, these contact pads acted as a DC-bias branch of the mixer and as its IF readout. The first titanium layer provides a better adhesion between the layers and the second one acts as a protection mask during the ion milling process.

Figure 2 shows the schematic of the experimental setup that was used to test the bandwidth and sensitivity of the mixers. The HEB mixer was precisely aligned with the fiber core under an optical microscope (Fig. 2, inset) and installed onto a cold plate of either a wet cryostat or closed-cycle cryocooler [we used a Gifford–McMahon
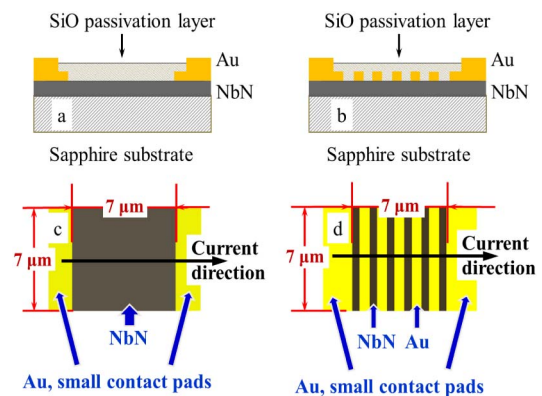

Fig. 1. Schematic representation of the HEB devices. (a) Cross section and (c) top view of the regular NbN bridge, (b) cross section and (d) top view of the HEB device with golden stripes atop.
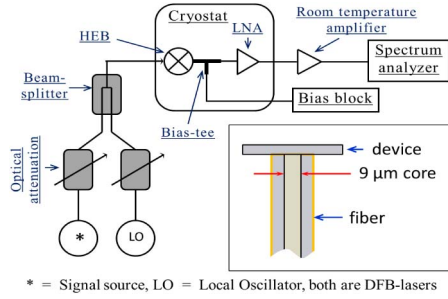
Fig. 2.   Principle schematic of the experimental setup. A bias-tee allows both to apply dc-biasing to the device and read the IF power, which is further amplified by both a cryogenic low noise amplifier (LNA) and a room temperature amplifier. An RF spectrum analyzer was used for the IF signal analysis. Inset shows coupling between the fiber waveguide and the HEB device.
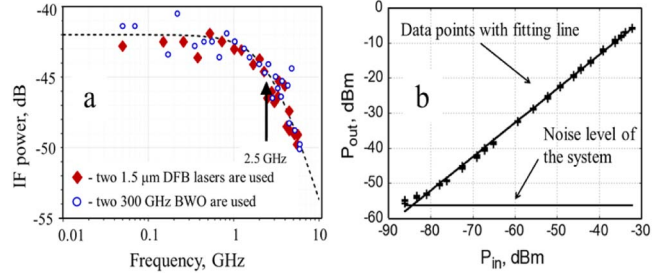

Fig. 3.   (a) Intermediate frequency bandwidth of the HEB mixer measured at the LO wavelength of 1.55 μm and compared to the IF bandwidth measurement performed at a conventional for the THz detection LO frequency of 300 GHz. To perform the latter measurement, two backward wave oscillators (BWO) were used. (b) Receiver dynamic range measured with the test signal power varied and was found to be more than 50 dB.

cryocooler from Janis, Inc. (www.janis.com)] along with a cold bias-tee and cryogenic low noise amplifier (LNA). First, we determined the IF bandwidth of the mixers. The gain bandwidth was measured by means of a standard frequency beating method with two CW sources [we used a couple of narrow-line fiber-coupled distributed feedback (DFB) lasers (www.furukawa.co.uk) irradiating at 1.55 μm]. The mixer was pumped to its operating point by applying power from the LO, which was one of the CW sources. The second CW source had its power-level strongly attenuated to mimic a signal. Both signals were coupled together with a fiber-optic beam splitter and then directed to the HEB device. To measure the HEB mixer IF bandwidth, we tuned the LO frequency by a slight change of the operating temperature of the DFB laser. The crucial requirement for this method is the LO power constancy, which was monitored both by the device current (which strongly depends on the LO power) and also directly by an optical power meter. The IF bandwidth of the HEB mixer is the result of the electron–phonon interaction time, which is determined by the material, and combined with diffusive processes due to the geometry. In addition, the phonon escape time from the film to substrate plays a role, which depends on the acoustical coupling of the NbN phonons to the substrate phonon bath. Given these processes, one should not expect that the IF bandwidth at IR frequencies will be different from the one at subterahertz frequencies. To confirm this statement, we measured the IF bandwidth of the same device at an LO frequency of 300 GHz. Both results are shown in Fig. 3(a). The good agreement proves our intuitive expectation and indicates that at both frequency regimes the same hot-electron processes are responsible for the mixing.

To further characterize the mixer performance, both the receiver dynamic range and its sensitivity were measured. Using a weak signal from the signal laser, we observed the IF output power P_{out}^{IF} as a function of the incident signal power $P_{\text{in}}^{\text{sign}}$. As shown in Fig. 3(b), the HEB mixer response was fully linear over a 50 dB range of power. The system sensitivity was determined with the well known Y-factor measurement. As a test signal source, we again used the attenuated signal of one of the lasers. First, we measured the signal laser power and then the IF output power from the mixer. After changing

the signal laser power by a slight change of the attenuation, the signal laser power and the IF output power were measured again. By setting the power of the signal laser low enough to not disturb the mixer operating point set by the LO, we eliminated the direct detection response [39], which often affects HEB mixer performance measurements. In the future, a more detailed analysis may be needed, similar to the one used in [40]. Assuming that the receiver output power is $P^{\text{out}} = G_{\text{sys}} \cdot (P^{\text{in}} + P_{\text{sys}})$, where G_{sys} is the system gain, P^{in} the input radiation power, and P_{sys} the noise power added by the system, the receiver noise spectral density can be expressed as $S_{\text{sys}} = [P_1^{\text{in}} - Y \cdot P_2^{\text{in}}]/[(Y - 1) \cdot B]$, where $Y = P_1^{\text{out}}/P_2^{\text{out}}$, P_1^{out}, and P_2^{out} are the receiver power outputs produced in response to the input signals with powers of P_1^{in} and P_2^{in} irradiated by the signal laser. From the measurements, we estimated the system noise figure to be about 25 dB (where the noise figure is NF = $10 \cdot lg(1 + S_{\text{sys}}/(k_B \cdot T_0))$ and $T_0 = 290$ K), and notably, it exceeded the quantum limit by only 10 dB, which is encouraging in line with the results obtained around 5 THz. To verify these results, the output noise density of the receiving system (i.e., with no test signal coming from the signal laser) was measured directly and normalized to the system gain. The same noise figure of the system was obtained. An analysis of the radiation absorption showed that the excess noise was most likely due to suboptimal coupling of the incident light to the NbN nanobolometer. Hence, by further improving the optical coupling of the noise figure of the receiver, we should be able to approach the quantum limit further.

In conclusion, we have developed a highly sensitive near-IR broadband fiber-optic coupled heterodyne receiver using a superconducting HEB that is suitable for numerous applications where a weak signal needs to be detected with a high spectral resolution. It has been shown that NbN HEB mixer can be operated successfully at IR wavelengths, where the incident photon energy is ~100 times larger than at the conventional terahertz frequency range. In addition, a novel "zebra" structure was implemented to enhance the incident radiation-to-NbN film coupling. The measured receiver noise figure was about 25 dB and only 10 dB higher than the limit set

by the quantum noise. Further improvement in light coupling to the NbN nanobolometer should be achievable by making use of a resonator structure or implementing an advanced optical antenna. A relatively wide IF bandwidth of about 2.5 GHz was observed, which was found to be identical to the one at 300 GHz thereby proving that hot-electron effects are determining the mixing process.

References

1. D. Sasselov, *The Life of Super-Earths: How the Hunt for Alien Worlds and Artificial Cells Will Revolutionize Life on Our Planet* (Basic Books, 2012).
2. J. D. Fraine, D. Deming, M. Gillon, E. Jehin, B. O. Demory, B. Benneke, S. Seager, N. K. Lewis, H. Knutson, and J. M. Désert, Astrophys. J. **765**, 127 (2013).
3. F. Fressin, G. Torres, F. Pont, H. Knutson, D. Charbonneau, T. Mazeh, S. Aigrain, M. Fridlund, C. E. Henze, T. Guillot, and H. Rauer, Astrophys. J. **745**, 81 (2012).
4. F. Hase, L. Wallace, S. D. McLeod, J. J. Harrison, and P. F. Bernath, J. Quant. Spectrosc. Radiat. Transfer **111**, 521 (2010).
5. D. Glenar, H. Käufl, D. Deming, T. Kostiuk, and M. J. Mumma, *Advances in Helio- and Astroseismology*, J. Christensen-Dalsgaard and S. Frandsen, eds. (Springer, 1987), pp. 481–484.
6. J. B. Altepeter, D. F. V. James, and P. G. Kwiat, *Quantum State Estimation. Lecture Notes in Physics*, M. Paris and J. Rehacek, eds. (Springer, 2004).
7. J. B. Altepeter, E. R. Jeffrey, and P. G. Kwiat, Adv. At. Mol. Opt. Phys. **52**, 105 (2005).
8. A. Lvovsky and M. Raymer, Rev. Mod. Phys. **81**, 299 (2009).
9. D. Huang, E. Swanson, C. Lin, J. Schuman, W. Stinson, W. Chang, M. Hee, T. Flotire, K. Gregory, C. Puliafito, and J. Fujimoto, Science **254**, 1178 (1991).
10. S. Chinn, E. Swanson, and J. Fujimoto, Opt. Lett. **22**, 340 (1997).
11. A. H. Hartog, in *Optical Fiber Sensors*, *Collected Papers of the International Conferences on Optical Fiber Sensors 1983–1997* (Optical Society of America, 1992), paper TH11.
12. R. Bernini, L. Crocco, A. Minardo, F. Soldovieri, and L. Zeni, Opt. Lett. **27**, 288 (2002).
13. T. Chen, K. P. Chen, Q. Wang, B. Zhang, and R. Chen, *Imaging and Applied Optics Technical Papers*, OSA Technical Digest (online) (Optical Society of America, 2012), paper STu3F.2.
14. T. Kostiuk and M. Mumma, Appl. Opt. **22**, 2644 (1983).
15. R. Schieder, G. Sonnabend, M. Sornig, P. Kroetz, and D. Stupar, "Observations with the tuneable heterodyne infrared spectrometer 'THIS'," in the *33rd International Conference on Infrared, Millimeter and Terahertz Waves*, Pasadena, California, USA, September 15–19, 2008.
16. https://www.astro.uni-koeln.de/this.
17. A. Klimchuk, A. Nadezhdinskii, Ya. Ponurovskii, Yu. Shapovalov, and A. Rodin, Quantum Electron. **42**, 244 (2012).
18. G. N. Gol'tsman, Infrared Phys. Technol. **40**, 199 (1999).
19. J. Kawamura, T. R. Hunter, C.-Y. E. Tong, R. Blundell, D. C. Papa, W. Peters, T. Wilson, C. Henkel, G. Gol'tsman, and E. Gershenzon, Astron. Astrophys. **394**, 271 (2002).
20. D. Marrone, R. Blundell, C.-Y. E. Tong, S. Paine, D. Loudkov, J. Kawamura, D. Lühr, and C. Barrientos, "Observations in the 1.3 and 1.5 THz atmospheric windows with the Receiver Lab Telescope," arXiv:astro-ph/0505273 (2005).
21. http://herschel.esac.esa.int/.
22. http://www.sofia.usra.edu/.
23. J. Kloosterman, D. Hayton, Y. Ren, T. Kao, J. Hovenier, J. Gao, T. M. Klapwijk, Q. Hu, C. Walker, and J. Reno, Appl. Phys. Lett. **102**, 011123 (2013).
24. S. Maslennikov, M. Finkel, S. Antipov, S. Polyakov, W. Zhang, R. Ozhegov, Yu. Vachtomin, S. Svechnikov, K. Smirnov, Yu. Korotetskaya, N. Kaurova, B. Voronov, and G. Gol'tsman, *Proceedings of the 17th International Symposium on Space Terahertz Technology* (National Radio Astronomy Observatory, 2006), pp. 177–179.
25. T. Wilson, K. Rohlfs, and S. Hüttemeister, *Tools for Radio Astronomy*, 5th ed. (Springer, 2009), pp. 97.
26. A. Semenov, G. Gol'tsman, and R. Sobolewski, Supercond. Sci. Technol. **15**, R1 (2002).
27. W. Zhang, P. Khosropanah, J. Gao, T. Bansal, T. M. Klapwijk, W. Miao, and S. Shi, J. Appl. Phys. **108**, 093102 (2010).
28. W. Zhang, P. Khosropanah, J. Gao, E. Kollberg, K. Yngvesson, T. Bansal, R. Barends, and T. M. Klapwijk, Appl. Phys. Lett. **96**, 111113 (2010).
29. A. E. Siegman, Appl. Opt. **5**, 1588 (1966).
30. I. Codreanu and G. D. Boreman, Microw. Opt. Technol. Lett. **29**, 381 (2001).
31. P. Bharadwaj, B. Deutsch, and L. Novotny, Adv. Opt. Photon. **1**, 438 (2009).
32. L. Novotny and N. van Hulst, Nat. Photonics **5**, 83 (2011).
33. A. Kawakami, S. Saito, and M. Hyodo, IEEE Trans. Appl. Supercond. **21**, 632 (2011).
34. X. Hu, E. Dauler, R. Molnar, and K. Berggren, Opt. Express **19**, 17 (2011).
35. L. Novotny, Phys. Rev. Lett. **98**, 266802 (2007).
36. H. Ekström, B. Karasik, E. Kollberg, and S. Yngvesson, IEEE Trans. Microwave Theor. Tech. **43**, 938 (1995).
37. I. Tretyakov, S. Ryabchun, M. Finkel, S. Maslennikov, A. Maslennikova, N. Kaurova, A. Lobastova, B. Voronov, and G. Gol'tsman, IEEE Trans. Appl. Supercond. **21**, 620 (2011).
38. A. Semenov, B. Günther, U. Böttger, H. W. Hübers, H. Bartolf, A. Engel, A. Schilling, K. Ilin, M. Siegel, R. Schneider, D. Gerthsen, and N. A. Gippius, Phys. Rev. B **80**, 054510 (2009).
39. Y. Lobanov, C.-Y. E. Tong, R. Blundell, and G. Gol'tsman, *Proceedings of the 20th International Symposium on Space Terahertz Technology* (National Radio Astronomy Observatory, 2009), pp. 282–287.
40. D. Hayton, J. R. Gao, J. W. Kooi, Y. Ren, W. Zhang, and G. de Lange, Appl. Phys. Lett. **100**, 081102 (2012).